Applied Magnetic Resonance (2020) 51:205–219
https://doi.org/10.1007/s00723-019-01157-1

Applied
Magnetic Resonance

ORIGINAL PAPER

Monitoring Lithology Variations in Drilled Rock Formations Using NMR Apparent Magnetic Susceptibility Contrast

Jonathan Mitchell[1]

Received: 1 July 2019 / Revised: 6 August 2019 / Published online: 6 February 2020

Abstract

Nuclear magnetic resonance (NMR) is a powerful technique for determining the petrophysical properties (porosity, permeability, and fluid mobility) of subsurface reservoirs through well logs, laboratory core analysis, or surface measurements of drill cuttings at the rig site. In well logging, NMR is considered a lithology-independent tool, but in surface measurements, it is possible to determine the apparent magnetic susceptibility contrast between the rock and a saturating liquid from a measure of the free induction decay. The magnetic susceptibility of the rock is influenced by paramagnetic minerals (iron and manganese oxides) and provides a simple method for detecting variations in lithology, particularly shale bands. Here, NMR measurements of apparent magnetic susceptibility contrast are obtained on a selection of core plugs, powdered rock, and drilled cuttings using a commercial bench top instrument, and shown to correlate to the iron content of the samples. This rapid and robust analysis complements the standard NMR petrophysical measurements and could be used to detect formation tops in near-real-time at the rig site.

1 Introduction

Lithological descriptions of rock, such as mineral content and grain texture, provide information on the age and depositional environment of subsurface formations [1]. As such, lithology is important in petroleum reservoir exploration and production, notably in the identification of formation tops (significant changes in lithology, e.g., on moving from a cap rock to reservoir) while drilling. Lithology is traditionally determined by a geologist using optical microscopy to inspect rock recovered at the surface, either as drill cuttings at the rig site (part of a standard mud-logging

Dr Jonathan Mitchell sadly passed away during the editorial processing of this, his last scientific paper. Proof reading was completed by Dr Edmund Fordham, whose email (fordham1@slb.com) coordinates are given for correspondence.

✉ Jonathan Mitchell

[1] Schlumberger Cambridge Research, High Cross, Madingley Road, Cambridge CB3 0EL, UK

service) or as cored samples (or prepared as thin sections) in the laboratory (routine core analysis service). Down-hole lithology can be determined from natural gamma-ray detection tools and logging-while-drilling (LWD) returns near-real-time characterization of the formation to guide directional drilling in deviated wells [2]. These logs provide clear distinction of shale bands containing absorbed uranium and thorium from sandstones, but identifying carbonate formations is unreliable due to their variable radioactive mineral content. The detailed lithology descriptions available through modern sophisticated mud-logging techniques tend to remain labor-intensive and may not be timely or determined with sufficient frequency to guide drilling operations [3, 4]. An alternative surface measurement of lithology, suitable for automation at the rig site to provide near-real-time answers, is magnetic susceptibility [5].

The magnetic susceptibility χ of a substance describes its ability to acquire a magnetic dipole moment when subjected to a magnetic field:

$$\mathbf{M} = \chi \mathbf{H} \tag{1}$$

where $\mathbf{M}$ is the sample magnetization and $\mathbf{H}$ is the imposed magnetic field. The temperature variation of χ for many paramagnetic substances is given by Curie's Law as:

$$\chi = \frac{C}{T} \tag{2}$$

where T is the absolute temperature and C is the Curie constant approximated as [6]:

$$C \simeq \frac{\mu_0 \mu^2}{3k_\mathrm{B}} N \tag{3}$$

where μ is the magnetic moment per atomic dipole, N is the number density of such dipoles, $\mu_0 = 1.257 \times 10^{-6}\,\mathrm{H\ m^{-1}}$ is the permeability of free space, and $k_\mathrm{B} = 1.38 \times 10^{-23}\,\mathrm{J\ K^{-1}}$ is the Boltzmann constant. Magnetic susceptibilities may be positive (paramagnetic) or negative (diamagnetic). Paramagnetism in subsurface formations derives predominantly from iron and manganese [7], whereas common minerals such as quartz and calcite are diamagnetic. Gross changes in lithology (formation tops) are, therefore, often easy to detect, particularly when moving between a weakly diamagnetic sandstone or limestone and a strongly paramagnetic shale [8–10].

Magnetic susceptibility is usually determined by means of a Gouy (or Evans) balance [11, 12] which measures the physical deflection of a permanent magnet, or a susceptibility bridge where the modulation in frequency of an alternating current (AC) induction field is measured [5]. The Evans balance is best suited to the measurement of dry powders and liquids, whereas a susceptibility bridge can be applied to powders or large samples depending on the instrument geometry. In core analysis, a susceptibility bridge is applied to dry competent plugs with a correction for the formation porosity ϕ. Although both instruments are small and portable, care must be taken due to their sensitivity to the local magnetic environment (e.g., steel construction, hand tools, etc.) and extensive sample preparation

may be required (e.g., drying plus an independent porosity measurement for core plugs and drill cuttings). Alternatively, magnetic susceptibility of rocks can be determined using an SQUID (superconducting quantum interference device) magnetometer as described in [13].

An alternative approach to measuring magnetic susceptibility is nuclear magnetic resonance (NMR) [14, 15]. In well logging, NMR provides a powerful tool for investigating petrophysical properties of the subsurface formation, such as porosity, permeability, identification of producible zones [16], and wettability [17]. NMR is marketed as a lithology-independent down-hole measurement, unlike other common techniques such as neutron porosity that require prior knowledge of the rock type for robust interpretation. Most NMR petrophysical interpretations, either down hole or in the laboratory, are based on analysis of the transverse relaxation time T_2 determined using the classic Carr–Purcell–Meiboom–Gill (CPMG) echo train experiment [18, 19]. Refocusing of the magnetization in a spin echo reduces the influence of molecular diffusion through magnetic field inhomogeneities. Interpretations based on the longitudinal T_1 relaxation time are insensitive to spatial variations in magnetic field [20]. In the absence of a refocusing spin echo, the free induction decay (FID) [21] of transverse magnetization approximately proceeds with an exponential rate constant:

$$\frac{1}{T_2^*} \approx \frac{1}{T_2} + \gamma \Delta\chi B_0 + \gamma \Delta B_0, \tag{4}$$

where γ is the gyromagnetic ratio, B_0 is the static magnetic field strength, ΔB_0 is the instrument-specific field inhomogeneity, and $\Delta\chi$ is the solid/liquid magnetic susceptibility contrast. The true transverse relaxation time T_2 is typically longer by orders of magnitude than T_2^* and so is ignored. The magnetic susceptibility varies in space and a strict exponential magnetization decay is observed only when the distribution of local field fluctuations is Gaussian [23]. To be rigorous, we should consider the volume-averaged integral of the magnetic field distortion $\int \gamma \Delta\chi(\mathbf{r}) B_0 \mathrm{d}V$. However, as this integral is challenging to calculate for a sample where the field fluctuations are not random [22], we use Eq. (4) based on empirical observations [25]. This equation will break down in the limiting cases of (1) large instrument field inhomogeneity, i.e., $\Delta B_0 \gg \Delta\chi B_0$ [26], (2) a non-Gaussian spin phase distribution caused by diffusion through large internal gradients [27], or (3) small pores of characteristic length ℓ_s that restrict the diffusion path of the liquid molecules [28]. If the distribution of local field fluctuations does not average to zero, then the linear field terms in Eq. (4) will give rise to a shift in the resonant frequency [24] as well as the spectroscopic line broadening described by $1/T_2^*$. However, in the present work, any such small-frequency shifts were masked by the inherent width of the spectra (short T_2^*) as a result of using low-field permanent magnets.

Equation (4) leads to an empirical measure of apparent magnetic susceptibility contrast defined as:

$$\begin{aligned}\Delta\chi_{\text{app}} &= \frac{\Delta\omega}{c_\chi\omega_0} \\ &= \frac{1}{\pi T_2^*}\cdot\frac{1}{c_\chi\gamma B_0} \\ &\approx \frac{1}{T_2^*}\cdot\frac{1}{\gamma B_0},\end{aligned} \tag{5}$$

where $\omega_0 = \gamma B_0$ is the Larmor frequency and $c_\chi \approx 0.3$ is an empirical scaling parameter [25] that conveniently cancels the factor π in the denominator. The NMR magnetic susceptibility contrast $\Delta\chi_{\text{app}}$ measured in rocks is subtly modified from the true magnetic susceptibility contrast $|\Delta\chi| = |\chi(\text{rock}) - \chi(\text{liquid})|$ due to the influence of pore size on the local magnetic field distortions, particularly if the pores are large ($\ell_s \geq 100\,\mu\text{m}$) or small ($\ell_s \leq 1\,\mu\text{m}$) [28]. In many cases, the magnetic susceptibility contrast between the rock mineral and saturating brine or oil is modest to large, and very large in iron-rich clays, e.g., chlorite [29]. Although the measurement of an FID is not practical with current *ex situ* well-logging tools due to the inherent ΔB_0 field inhomogeneity of the magnets, it is possible to determine $\Delta\chi_{\text{app}}$ using commercial bench top NMR instruments, readily available with field strengths up to $B_0 \sim 0.5\,\text{T}$. Such instruments are appropriate for laboratory core analysis or rig site analysis of drill cuttings, being portable and robust to changes in the external magnetic environment, and minimal sample preparation is required.

Rig site NMR is not a new concept. Numerous studies are to be found in the literature dating back to the 1980s [30] comparing porosity measurements from cuttings to core plugs or well logs in both conventional and unconventional formations. However, surface NMR has never achieved commercial success as a mud-logging technology due to unreliable results; a limitation that was not resolved through continued improvements to the magnet technology [31, 32]. In recent works, it was demonstrated that the chronic problem of gross overestimation in porosity is mitigated by robust and repeatable sample-handling procedures [33–35]. Petrophysical characterization of the rock still requires competent cuttings of sufficient size (e.g., 20–100 grains) to reflect the formation microstructure [36]. NMR apparent magnetic susceptibility contrast, on the other hand, can be determined on cuttings of any size and even unconsolidated grains. These measurements could provide near-real-time detection of formation tops while drilling.

Previously, NMR magnetic susceptibility measurements have been used to calibrate T_2 cut-offs in relaxation time distributions of liquid-saturated rocks [37] and to correct water saturation measurements in porous iron ore [38]. T_2^* has been used to assess the strength of "internal gradients" in rocks [39–41] and distributions of T_2^* correlated against T_1 have been used as an indicator of formation heterogeneity [42]. Magnetic susceptibility is also a well-known contrast mechanism in medical imaging [43, 44] and the single-exponential T_2^* decay observed in rocks (and many other porous materials) is convenient for quantitative single-point imaging (SPI) [25, 45].

In this paper, the utility of NMR apparent magnetic susceptibility contrast as an indicator of lithology is demonstrated through measurements of powdered rock and core plugs, and drill cuttings generated from a subsurface formation. The physical

rock properties are described in Sect. 2.1 and the results of conventional magnetic susceptibility measurements are presented in Sect. 2.2. The NMR technique is introduced in Sect. 2.3 and the measured apparent magnetic susceptibility contrasts are discussed in Sect. 3.

2 Materials and Methods

2.1 Rock Samples

A selection of outcrop rocks was prepared as powders and cylindrical core plugs (diameter × length: 38 × 50 mm) for analysis by NMR and conventional magnetic susceptibility measurement. The powdered rock was prepared by crushing a small quantity of each formation in a planetary ball mill (PM100, Retsch, Germany) using an agate cup and grinding spheres. The ball mill components were washed thoroughly with deionized water and acetone after each cycle to prevent cross contamination of samples. Details of the outcrop formations, including lithological classification based on thin-section analysis, are listed in Table 1. Conventional magnetic susceptibility measurements were performed on the dry samples.

For the NMR measurements, the rock powders (approximately 10 g of each) were suspended in deionized water and centrifuged at 500 RPM for 60 min in a low-speed bench top centrifuge (LMC-3000, Grant Instruments, UK) to produce a dense slurry. The excess liquid was carefully aspirated from the tubes. The sealed centrifuge tubes were placed directly in the NMR magnet using a custom sample holder. The water content of the wet powders was not assessed here, although in principle, this is a trivial parameter extracted from the total NMR signal and sample mass. Water absorption depends on the wettability (mineralogy and chemistry) of the formation, and so could potentially provide additional information. Dissolution of minerals (e.g., iron oxides) into the water is another detail, beyond the scope of the current work, that could be explored.

The core plugs were vacuum-saturated with low-salinity brine [46] and stored under brine between measurements. For the duration of the NMR measurements, the core plugs were wrapped in plastic film and placed in a PTFE cup.

Drill cuttings produced at the Cameron Test Facility (CTF, Texas, USA) were shipped to a laboratory for analysis [35]. The cuttings depth (provenance) was estimated from the volumetric mud flow rate. The cuttings were taken directly from the shale shaker and sealed in plastic bottles for transport. On arrival at the laboratory, the cuttings were recovered from the bottles and rinsed under tap water to remove water-based mud solids (barite weighting agent and loss control material). The cuttings were sieved wet and a fraction in the size range 1 to 3 mm (18 − 6 mesh) retained for NMR assay. The cleaned cuttings were centrifuged under perfluorinated oil at $\Omega = 31\,\mathrm{rad\,s^{-1}}$ (300 rpm) for $t = 600\,\mathrm{s}$ on a low-speed bench top centrifuge and measured by NMR without further preparation. Neutron porosity and natural gamma-ray logs were obtained in an adjacent (but not identical) well for comparison.

Table 1 Properties of conventional outcrop formations

Formation	Abbr.	Lithology	Classification	ϕ/p.u.	Fe/%
Sandstones					
Bentheimer	BN	Sandstone	Subarkose	24	0.03
Birchover (a)	BRa	Millstone grit	Subarkose	17	0.38
Birchover (b)	BRb	Millstone grit	Subarkose	15	0.50
Berea (a)	BXa	Sandstone	Subarkose	19	0.73
Berea (b)	BXb	Sandstone	Subarkose	20	0.50
Berea (c)	BXc	Sandstone	Subarkose	24	0.35
Clashach (a)	CLa	Sandstone	Subarkose	19	0.07
Clashach (b)	CLb	Sandstone	Subarkose	20	0.07
Lazonby Red	LA	Sandstone	Subarkose	14	0.27
Ohio Blue	OB	Sandstone	Quartz wacke	17	1.59
Stancliffe	ST	Millstone grit	Subarkose	13	0.76
Carbonates					
Doulting	DO	Limestone	Bioclastic grainstone	21	0.45
Estillades	ES	Limestone	Bioclastic grainstone	30	0.04
Indiana	IN	Limestone	Bioclastic grainstone	19	0.07
Ketton	KT	Limestone	Oolitic grainstone	24	0.44
Marble	MB	Limestone	Crystalline carbonate	0	0.07
Portland	PT	Limestone	Bioclastic ooliticgrainstone	21	0.05
Rocharon	RO	Limestone	Bioclastic intraclastic grainstone	0	0.07
Stoke Ground	SG	Limestone	Bioclastic oolitic packstone	21	0.58
Stevns Klint	SK	Chalk	Mudstone	50	0.02
Silurian	SL	Dolomite	Crystalline carbonate	19	0.14

Lithological descriptors were determined from thin-section images (Corex, UK). Porosity values (expressed in porosity units, p.u.) were determined from the total NMR signal amplitude of the brine-saturated core plugs. The iron content was determined using X-ray elemental analysis of the powdered rock (expressed as a percentage of detected elements)

The magnetic susceptibility was slightly different for the deionized water, tap water, and brine used to saturate the various samples (powders, cuttings, and plugs) for NMR measurement, and so, a small offset was expected between the sets of measurements. The variation between the liquid magnetic susceptibilities ($\sim 10^{-7}\,\mathrm{cm^3\,g^{-1}}$) was considered small compared to the solid/liquid contrast ($\sim 10^{-6}\,\mathrm{cm^3\,g^{-1}}$), except for some of the diamagnetic outcrop rocks where the susceptibility contrast was near zero.

2.2 Conventional Magnetic Susceptibility Measurements

Magnetic susceptibility may be expressed in terms of volume χ_v, mass χ_g, or molarity χ_M. The unit system used to express magnetic susceptibility can be rationalized (mksA) or unrationalized (cgs-emu), with a factor 4π difference. Care must be taken to explicitly state the unit system, especially in the case of the dimensionless volume

susceptibility, to avoid confusion. Here, reference to rationalized units is achieved by inclusion of the 4π multiplier [43].

Absolute magnetic susceptibilities of the outcrop rocks were determined using (a) a Sherwood Scientific Mk1 balance for the dry powders and (b) a Bartington Instruments MS2C magnetic susceptibility meter for the dry core plugs. The Sherwood Scientific Mk1 instrument is based on the Evans balance [12], wherein the deflection of permanent magnet due to the presence of a powder or liquid sample is measured. The Bartington Instruments MS2C meter uses an AC induction loop [5] to determine the magnetic susceptibility of a large sample, such as a rock core. The liquid–solid mass susceptibility contrast $|\Delta\chi_g| = |\chi_g(\text{rock}) - \chi_g(\text{water})|$ was obtained by assuming a literature value of $\chi_g(\text{water}) = -0.72 \times 10^{-6}\,\text{cm}^3\,\text{g}^{-1}$. An experimentally determined magnetic susceptibility of water was close to the expected literature, but found to vary between samples, possibly due to the presence of dissolved (paramagnetic) oxygen.

The magnetic susceptibility distribution for the outcrop rocks is shown in Fig. 1a. An instrument offset, determined by measurement of reference samples, was removed from these data. The rocks generally have low magnetic susceptibilities compared to typical reservoir formations [39], with an obvious extreme case being Ohio Blue. Even over this limited range, there is a strong positive correlation between the measured magnetic susceptibility and the iron content obtained from elemental analysis, see Fig. 1b. This correlation breaks down only for the samples with very low iron content, and especially the diamagnetic formations. The state of the iron has not been considered here (i.e., FeO or Fe_2O_3) and these oxides have different magnetic susceptibilities. Other paramagnetic species, such as manganese oxide, present in low (< 100 ppm) quantities were also not considered in this comparison. The strong positive correlation observed indicates that iron is the dominant source of paramagnetism in these samples. A comparison of the χ_g values obtained for the outcrop formations on the Sherwood Instruments Mk1 balance (powders) and the Bartington Instruments MS2C meter (core plugs) is shown in Fig. 1c. The core-plug values were corrected to account for the formation porosity, see Table 1, according to $\chi_g = \phi\chi_v/\rho$ using the mineral (grain) density. A reasonable correlation is observed between the sets of values obtained on the two independent instruments. There is significant scatter about the equality (dashed) line, but there is no consistent drift to suggest an offset in either data set. Repeat measurements gave consistent results and experimental error bars equivalent to the size of the plot markers. The degree of scatter is attributed to the different sample volumes measured. The Mk1 balance accommodates only a small powder sample ($\sim 0.16\,\text{cm}^3$ [43]), whereas the MS2C meter averages over the plug volume ($\sim 56\,\text{cm}^3$). The small powdered rock sample may not be representative of the larger plug volume in heterogeneous formations. The two independent sets of data are considered equivalent despite the differences in representative sample volume and methodology.

2.3 NMR Measurements

For petrophysical analysis of liquid-saturated conventional rock cores (sandstones and carbonates), it is considered mandatory to use low-field NMR equipment to obtain quantitative porosity and permeability estimates from T_2 relaxation

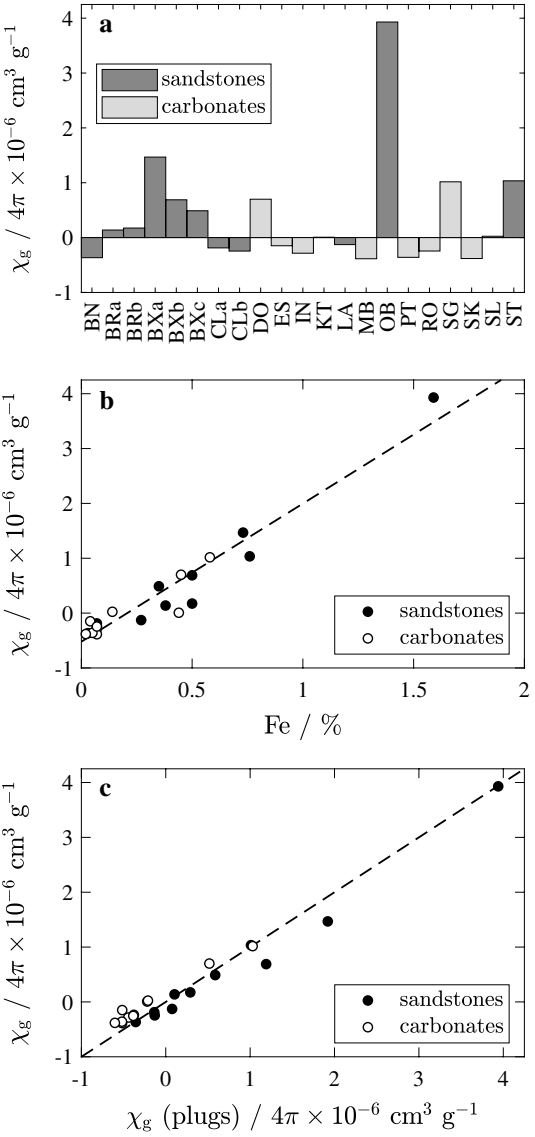

Fig. 1 Conventional magnetic susceptibility measurements of outcrop rocks. **a** Mass magnetic susceptibilities measured on powders using the Sherwood Scientific Mk1 susceptibility balance. Positive values indicate paramagnetism and negative values indicate diamagnetism. **b** Correlation between mass magnetic susceptibility and iron content. The iron content is expressed as a fraction of X-ray detected elements. The dashed line indicates a linear best fit to the data. **c** Comparison of mass magnetic susceptibility determined on core plugs using the Bartington Instruments MS2C magnetic susceptibility meter (abscissa) and powders using the Sherwood Scientific Mk1 susceptibility balance (ordinate). The dashed line indicates equality between the independent measurements

time distributions [47]. Typically, a resonant frequency of $f_0 \sim 2\,\text{MHz}$ for ^1H ($B_0 \approx 50\,\text{mT}$) is selected to minimize the influence of diffusion in internal gradients arising from the solid/liquid magnetic susceptibility contrast. This paradigm shifts for unconventional organic shale formations where higher field magnets improve fluid typing and enable detection of the solid kerogen [48]. Bench top instruments offering $f_0 \approx 23\,\text{MHz}$ for ^1H ($B_0 \approx 0.5\,\text{T}$) are now used routinely for laboratory analysis of unconventional shale formations and most commercial

systems of this field strength can accommodate small rock samples such as drill cuttings.

As T_2^* scales inversely with magnetic field strength from Eq. (4), stronger magnets provide a more sensitive measurement of the apparent magnetic susceptibility contrast (i.e., $\Delta\chi B_0$ increases, while ΔB_0 remains constant). This relation runs counter to the prevalent wisdom that NMR measurements of conventional rock formations be performed at low resonant frequencies. Of course, there is an inherent upper limit on the magnet strength as T_2^* will eventually become so short as to be undetectable at higher field strengths.

All the NMR measurements reported here were performed on an Oxford Instruments "Rock Core Imager" magnet at $f_0 = 12.9$ MHz for ^{1}H ($B_0 = 0.3$ T) as a compromise between the usual upper and lower ranges of field strength available on commercial bench top hardware. The capabilities of this particular instrument were reviewed in [49]. Wet rock powders and cuttings were measured using a 23 mm diameter radio frequency (rf) probe; brine-saturated core plugs were measured using a 53 mm diameter rf probe. The static magnetic field was adjusted by a combination of mechanical and electric shims to achieve a spectral line width for bulk water better than 10 ppm full-width-half-maximum (FWHM) in all cases. The magnetic field was more uniform across the sensitive region of the smaller probe. Both probes were fitted with an active damping feedback preamplifier (MRF Innovations, UK) to improve the signal-to-noise ratio (SNR) and probe response time. The rf pulses were supplied by a 500 W amplifier (Tomco, Australia) and typical 90° rf pulse durations were $t_{90} = 7$ µs for the 23 mm probe and $t_{90} = 15$ µs for the 53 mm probe.

Each FID contained 8192 data points acquired with a dwell time of 10 µs. A fluorine-suppression digital filter [50] was used to prevent signal contamination from PTFE components in the probe body and sample tubes. A recycle delay of 8 s was allowed between every scan to ensure full recovery of the longitudinal magnetization and 32 repeat scans were summed during acquisition to improve the SNR and accommodate the rf phase cycle. The total measurement time of each FID was approximately 4 min. The same protocol was applied to all the samples. The apparent magnetic susceptibility contrast was obtained according to Eq. (5) by fitting the FID with a single-exponential function of the form:

$$M(t) = M(0)\exp\left\{-\frac{t}{T_2^*}\right\}, \tag{6}$$

where t is the experiment time and M is the observed magnetization (signal). The total magnetization $M(0)$ was used to estimate the porosity of the core plugs (see Table 1) and cuttings (see [35]) by reference to a bulk water sample of known volume.

3 Results and Discussion

The NMR apparent magnetic susceptibility value for the outcrop rock powders is shown in Fig. 2a. It is important to note that the NMR measurement delivers only the magnitude of the susceptibility contrast and so any sense of paramagnetism or diamagnetism in the formation is lost. Nevertheless, it is possible to distinguish large changes between the rock samples. For example, the Ohio Blue sample still stands out as having a significantly higher (paramagnetic) susceptibility than any of the other rocks. As diamagnetic rocks tend to have low (negative) magnetic susceptibilities, it is reasonable to assume that all the formations exhibiting $\Delta\chi_{\text{app}} > 1 \times 10^{-6}\,\text{cm}^3\,\text{g}^{-1}$ are paramagnetic (a rule-of-thumb based on empirical observation). The NMR apparent magnetic susceptibility measurements on powders and plugs are compared in Fig. 2b. Note that not all the formations could be measured as plugs. The samples with zero porosity (Marble, Rocharon; see Table 1) could only be measured as powders and so are not included in this comparison. There is general agreement, with a significant scatter about the equality line for the samples with low magnetic susceptibility contrasts but no clear shift to suggest an offset in

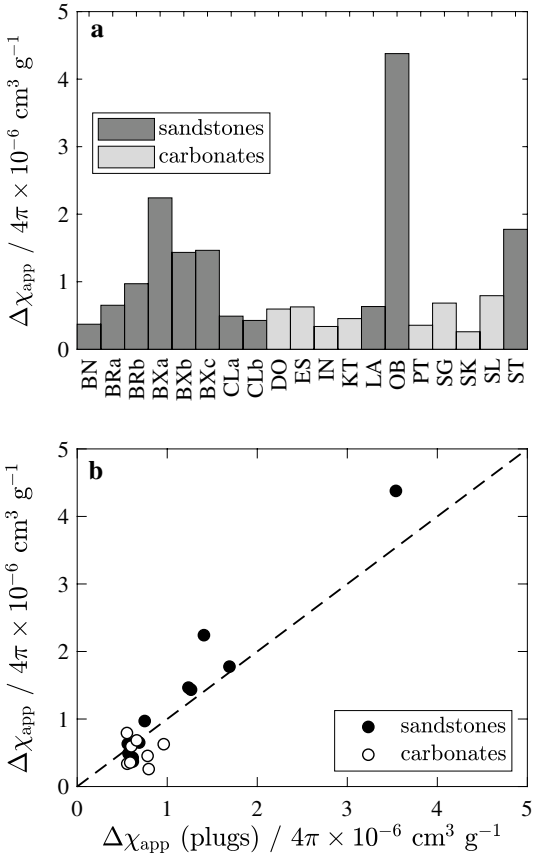

Fig. 2 NMR apparent magnetic susceptibility measurements of outcrop rocks. **a** Apparent mass magnetic susceptibility contrasts measured on wet powders. **b** Comparison of NMR apparent magnetic susceptibility contrasts measured on brine-saturated plugs (abscissa) and wet powders (ordinate). The dashed line indicates equality between the two sample sets

either measurement. It is interesting to note that the measured apparent susceptibility contrast of Ohio Blue is substantially lower in the plug than in the powder. This formation is characterized by small pores ($\ell_s \sim 1\,\mu m$), and in the competent plug, the NMR signal attenuation due to diffusion is reduced due to the restricting geometry (the "motional averaging" regime [51]). Consequently, the observed T_2^* relaxation time is longer than would be expected based on simple magnetostatics assumptions [28]. In the powder, this pore structure has been destroyed, removing the influence of restricted diffusion. The same effect is observed in the tightest Berea formation (BXa) with a similar nominal pore size. The NMR measurements of powders are considered more reliable for determining the apparent magnetic susceptibility contrast where the confounding influence of pore geometry is removed. In addition, for the rocks with a high iron content, the individual grains may have surface hematite and subsurface magnetite due to preferential surface oxidation. The oxidation states of iron exhibit very different magnetic susceptibilities ($+9.8 \times 10^{-5}\,cm^3\,g^{-1}$ for Fe_2O_3 and $+9.2 \times 10^{-2}\,cm^3\,g^{-1}$ for Fe_3O_4). Crushing the rock to powder will potentially expose the magnetite, thereby increasing the apparent magnetic susceptibility contrast of the powders compared to the plugs.

Good agreement was found between the NMR apparent magnetic susceptibility contrast and the Sherwood Mk1 balance measurements of the rock powders, see Fig. 3a. Except for two obvious outliers, the carbonate formations Doulting and Stoke Ground (rare examples of paramagnetic carbonates), the NMR measurement of susceptibility contrast agrees well with the traditional measurement. A strong correlation is also observed between the NMR apparent magnetic susceptibility contrast of the powdered sandstones and the iron content of the formations in Fig. 3b. The correlation between mineral magnetic susceptibility and iron content determined from the conventional measurements (dashed line in Fig. 1b) predicts the NMR response for the sandstones extremely well, albeit shifted by the mass magnetic susceptibility of water (dashed line in Fig. 3b). However, no strong correlation is observed for the carbonate formations, and three outliers are evident (all with Fe ≈ 0.5 %). Note that the majority of the carbonate samples are diamagnetic (see Fig. 1a), but this distinction is lost in the NMR measurement. The water could be replaced with a weakly paramagnetic solution to provide a second point of reference and hence determine the sign of the absolute magnetic susceptibility. This approach was not attempted here and would considerably complicate analysis of reservoir formations as typical NMR doping agents can chemically interact with the rock minerals [52]. Overall, it is clear from Fig. 3 that the NMR measurement is sufficiently sensitive to indicate changes in lithology during drilling and detect formation tops, especially where distinct changes in mineralogy occur such as a clay-rich shale bands.

The results of the NMR cuttings analysis are overlaid on the well logs in Fig. 4 (middle). The measured apparent magnetic susceptibility contrasts were adjusted using the neutron porosity and density values at comparable depths. These laboratory results generally follow the trends observed in the gamma-ray log. Above 610 m, the formation contained a significant clay fraction, corresponding to a high gamma-ray reading (~ 100 API), low bulk density, and high porosity. The apparent magnetic susceptibility contrast values were high in this region, consistent

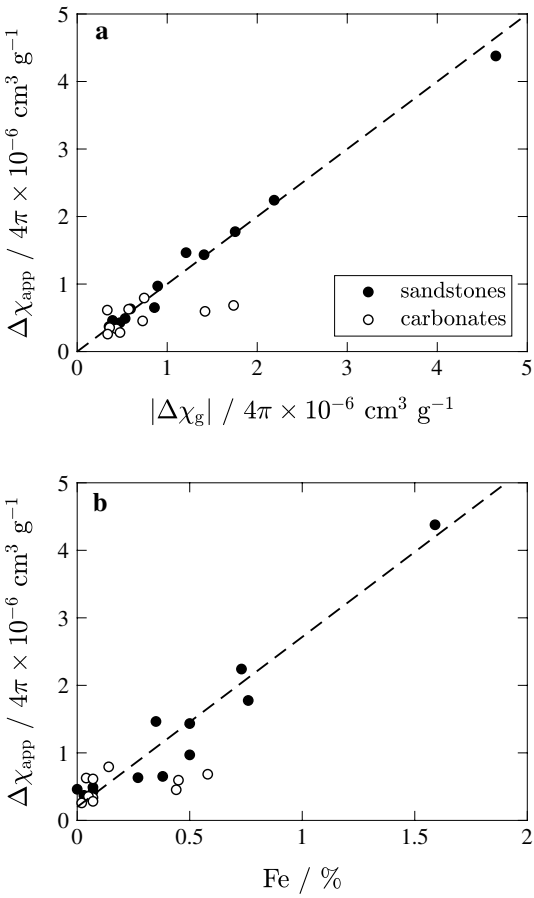

Fig. 3 Comparison of NMR apparent magnetic susceptibility measurements of wet outcrop rock powders to **a** conventional (mass) magnetic susceptibility contrast $|\Delta\chi_g|$ and **b** iron content. In **a**, the dashed line indicates equality between the two measurements. In **b**, the iron content is expressed as a fraction of X-ray detected elements. The dashed line is a linear best fit to the conventional magnetic susceptibility data (see Fig. 1b) adjusted by the mass magnetic susceptibility of water. The legend applies to both plots

with a significant iron content. Between 610 and 660 m, the formation was sandy leading to a reduced but still high apparent magnetic susceptibility contrast. Below 660 m, where the formation was increasingly dominated by limestone, the apparent magnetic susceptibility contrast decreased further. Very low values were observed around 850 m, suggesting another slight change in lithology that was not obvious from the gamma-ray log. The NMR data presented here are sparse, preventing detailed comparison to the gamma-ray and mineral logs, and there is an inherent uncertainty on the cuttings depth (on the order of several meters). Notwithstanding the limitations of this study, the changes in NMR apparent magnetic susceptibility contrast do correlate to the expected changes in formation and the measurement could be used to identify formation tops if the spatial resolution (frequency of cuttings collection) was improved. It is worth noting that the NMR measurement also delivered porosity and permeability information (as described in [35]) and so offers combined petrophysical and lithological indicators for the reservoir.

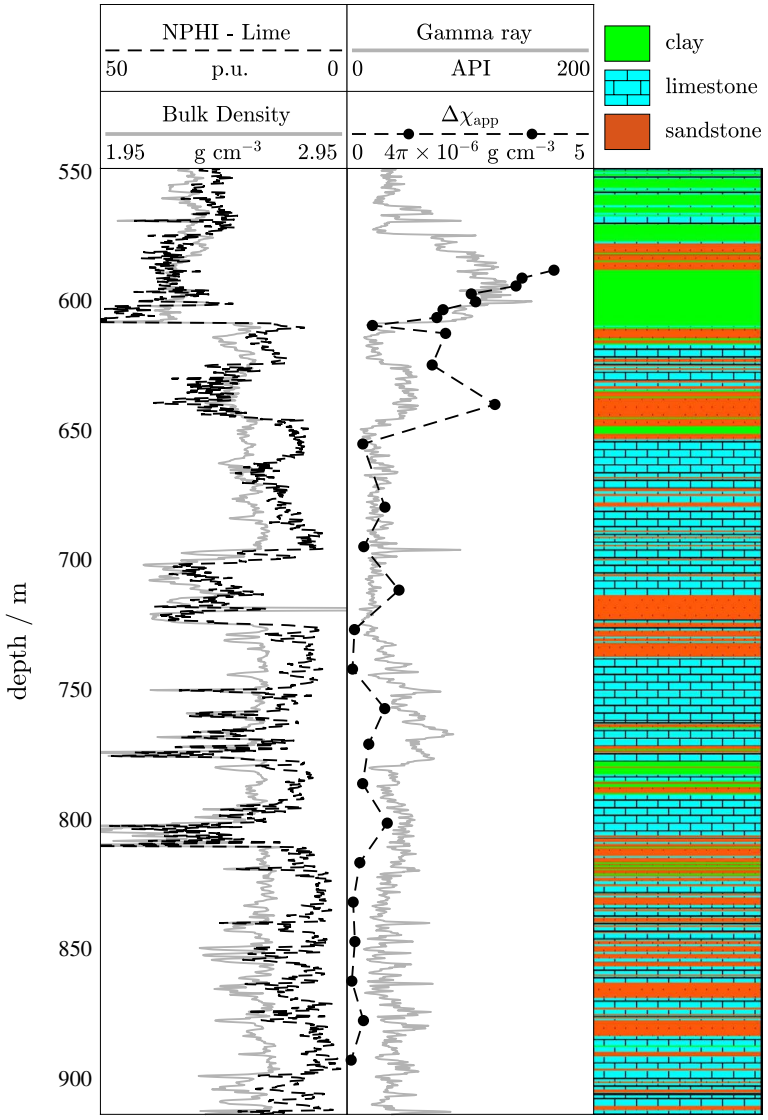

Fig. 4 Comparison of NMR cuttings analysis and logs for the CTF well. Left: neutron porosity (black dashed line) and formation density (gray line) well logs. Middle: NMR apparent magnetic susceptibility contrast (black dots with dashed connecting line) overlaid on the natural gamma-ray (gray line) well log. Right: a mineralogical interpretation of dominant rock type. The well-log data were presented previously in [35]

4 Conclusions

The magnetic susceptibility of a subsurface rock is a useful indicator of mineralogical variations in the formation. The magnetic susceptibility of the rock is influenced

by paramagnetic minerals (iron and manganese oxides) and provides a simple method for detecting variations in lithology, particularly clay-rich shale bands. However, conventional instrumentation for measuring magnetic susceptibility is sensitive to the local magnetic environment (e.g., structural steel, hand tools, etc.), demanding regular and careful calibration, and significant sample preparation is required. NMR offers an alternative methodology, being able to provide an apparent magnetic susceptibility contrast in liquid-saturated rocks with minimal sample preparation. Low-field bench top NMR instruments are robust to changes in the local magnetic environment and hence are appropriate for deployment at the rig site for near-real-time surface measurements of drill cuttings or core. In well logging, NMR is considered a lithology-independent tool, but in surface measurements, it is possible to determine an apparent magnetic susceptibility contrast from a free induction decay (FID). Here, NMR measurements of core plugs, powdered rock, and drilled cuttings were performed on a commercial bench top instrument. The apparent magnetic susceptibility contrast of outcrop rock formations correlated well to conventional magnetic susceptibility measurements and the iron content of the minerals. A magnetic susceptibility surface log was generated from the drill cuttings measurements and gross variations in lithology were identified in agreement with a corresponding natural gamma-ray well log. The NMR measurement of apparent magnetic susceptibility contrast is rapid and robust, sufficiently sensitive to detect formation tops, and complementary to standard NMR analyses (porosity, permeability). Through the addition of a simple FID measurement, a laboratory or rig site NMR service has the potential to provide combined petrophysical and lithological indicators in reservoir formations.

Acknowledgements Kaspars Karlsons is thanked for measuring the absolute magnetic susceptibility of the rock powders and core plugs. Mauro Caresta (Schlumberger Cambridge Research) organized collection of cuttings from the Cameron Test Facility. Edmund Fordham (Schlumberger Cambridge Research) is thanked for discussions on magnetic susceptibility units and measurements. Schlumberger is thanked for supporting this work.

References

1. A. Whittaker, *Mud Logging Handbook* (Prentice Hall, Upper Saddle River, 1991)
2. S. Bargach, I. Falconer, C. Maeso, J. Rasmus, T. Bornemann, R. Plumb, D. Codazzi, K. Hodenfield, G. Ford, J. Hartner, B. Grether, H. Rohler, Schlumberger Oilfield Rev. **12**, 58 (2000)
3. T. Loermans, M. Kanj, C. Bradford, in *Proceedings of the SPE Technical Symposium* (Dhahran, Saudi Arabia, May 14–16, 2005), SPE paper SPE-106324
4. T. Loermans, F. Kimour, C. Bradford, K. Bondabou, A. Marsala, in *Proceedings of the SPWLA 53rd Annual Logging Symposium* (Cartagena, Columbia, June 16–20, 2012), Paper SPWLA-2012-184
5. D. Collinson, *Methods in Rock Magnetism and Palaeomagnetism: Techniques and Instrumentation* (Chapman & Hall, New York, 1983)
6. C. Kittel, *Introduction to Solid State Physics* (Wiley, New York, 1953)
7. A. Perez-Perez, H. Romero, L. D'Onofrio, Geophys. **81**, J35 (2016)
8. D. Potter, Petrophysics **48**, 191 (2007)
9. M. Mena, A. Walther, Geol. Soc. Lond. Special Pubs. **371**, 217–228 (2012). https://doi.org/10.1144/SP371.14
10. A. Ali, D. Potter, A. Tugwell, in *Proceedings of the Society of Core Analysts Annual Symposium* (St Johns, Newfoundland, Canada, 16–21 August 2015, 2015) Paper 036

11. L. Mulay, *Physical Methods of Chemistry*, vol. 1 (Interscience, New York, 1972)
12. D. Evans, J. Phys. E Sci. Instrum. **7**, 247 (1974)
13. P. Connolly, W. Yan, D. Zhang, M. Mahmoud, M. Verrall, M. Lebedev, S. Iglauer, P. Metaxas, E. May, M. Johns, J. Petrol. Sci. Eng. **175**, 985 (2019)
14. G. Feher, W. Knight, Rev. Sci. Instrum. **26**, 293 (1955)
15. K. Frei, H. Bernstein, J. Chem. Phys. **37**, 1891 (1962)
16. R. Kleinberg, Concept. Magn. Reson. **342**, 13 (2001)
17. A. Valori, G. Hursan, S. Ma, Petrophysics **58**, 352 (2017)
18. H. Carr, E. Purcell, Phys. Rev. **94**, 630 (1954)
19. S. Meiboom, D. Gill, Rev. Sci. Instrum. **29**, 668 (1958)
20. K. Washburn, C. Eccles, P. Callaghan, J. Magn. Reson. **194**, 33 (2008)
21. E. Hahn, Phys. Rev. **77**, 297 (1950)
22. N. Fatkullin, Sov. Phys. JETP **74**, 833 (1991)
23. D. Grebenkov, Rev. Mod. Phys. **79**, 1077 (2007)
24. S. Majumdar, J. Gore, J. Magn. Reson. **78**, 41 (1988)
25. Q. Chen, A. Marble, B. Colpitts, B. Balcom, J. Magn. Reson. **175**, 300 (2005)
26. E. Fukushima, S. Roeder, *Experimental Pulse NMR: A Nuts and Bolts Approach* (Addison-Wesley Publishing Company, Reading, 1981)
27. T. de Swiet, P. Sen, J. Chem. Phys. **100**, 5597 (1994)
28. J. Mitchell, T. Chandrasekera, L. Gladden, J. Chem. Phys. **132**, 244705 (2010)
29. M. Hürlimann, A. Matteson, J. Massey, D. Allen, E. Fordham, F. Antonsen, H. Rueslatten, Petrophysics **45**, 414 (2004)
30. E. Nigh, M. Taylor, Can. Well Log. Soc. J. **13**, 45 (1984)
31. K. Mirotchnik, S. Kryuchkov, K. Strack, in *Proceedings of the SPWLA 45th Annual Logging Symposium* (Noordwijk, The Netherlands, June 6–9, 2004), Paper SPWLA-2004-MM
32. Z. Wang, Y. Martinez, K. Strack, G. Yu, in *Proceedings of the SPWLA 48th Annual Logging Symposium* (Austin, Texas, United States, June 3–6, 2007), Paper SPWLA-2007-X
33. M. Dick, D. Green, T. Kenney, D. Veselinoivc, J. Tallarita, M. Smith, in *Proceedings of the Society of Core Analysts Annual Symposium* (Vienna, Austria, 28 August – 1 September 2017, 2017) Paper 013
34. K. Fellah, S. Utusuzawa, Y. Song, R. Kausik, Energy Fuels **32**, 7467 (2018)
35. J. Mitchell, A. Valori, E. Fordham, J. Petrol. Sci. Eng. **174**, 351 (2019)
36. D. Georgi, T. Loermans, SPWLA Today **1**, 14 (2018)
37. B. Nicot, P. Ligneul, M. Akbar, US patent 9423365 B2, Granted: 23 Aug 2016
38. M. Carroll, K. O'Neill, N. Bristow, T. Hopper, S. Vogt, M. Johns, E. Fridjonsson, Min. Eng. **122**, 211 (2018)
39. M. Hürlimann, J. Magn. Reson. **131**, 232 (1998)
40. R. Lewis, J. Seland, J. Magn. Reson. **263**, 19 (2016)
41. J. Mitchell, T. Chandrasekera, M. Johns, L. Gladden, E. Fordham, Phys. Rev. E **81**, 026101 (2010)
42. J. Mitchell, J. Magn. Reson. **240**, 52 (2014)
43. J. Schenck, Med. Phys. **23**, 815 (1996)
44. E. Haacke, R. Brown, M. Thompson, R. Vankatesan, *Magnetic Resonance Imaging: Physical Principles and Sequence Design* (Wiley, New York, 1999)
45. M. Peyron, G. Pierens, A. Lucas, L. Hall, G. Potter, R. Stewart, D. Phelps, Magn. Reson. Imaging **12**, 295 (1994)
46. J. Mitchell, J. Staniland, R. Chassagne, E. Fordham, Transp. Porous Med. **94**, 683 (2012)
47. C. Straley, D. Rossini, H. Vinegar, P. Tutunjian, C. Morris, Log Anal. **38**, 84 (1997)
48. M. Fleury, M. Romero-Sarmiento, J. Petrol. Sci. Eng. **137**, 55 (2016)
49. J. Mitchell, E. Fordham, Rev. Sci. Instrum. **85**, 111502 (2014)
50. A. Valori, J. Mitchell, E. Fordham, Concept. Magn. Reson. **46B**, 202 (2017)
51. M. Hürlimann, K. Helmer, T. de Swiet, P. Sen, C. Sotak, J. Magn. Reson. Ser. A **113**, 260 (1995)
52. J. Mitchell, J. Staniland, E. Fordham, Petrophysics **54**, 349 (2013)